JOURNAL OF MATERIALS SCIENCE: MATERIALS IN MEDICINE **17** (2006) 95 – 104

Zinc phosphate as versatile material for potential biomedical applications Part II

L. HERSCHKE, I. LIEBERWIRTH*, G. WEGNER
Max Planck Institute for Polymer Research, Ackermannweg 10, D-55128 Mainz, Germany
E-mail: lieberw@mpip-mainz.mpg.de

Surface chemical reactivity of two modifications of synthetic zinc phosphate tetrahydrate (α- and β-form of Hopeite, α-,β-ZPT) has been studied by selective chemical and e-beam etching in presence of diluted phosphoric acid and ammonia by Scanning Electron Microscopy (SEM) and microelectrophoresis (zeta potential measurements) in correlation with the corresponding bulk properties and crystal size distributions. The subtitle crystallographic differences between α-and β-ZPT originating from a unique hydrogen bonding pattern, induce drastic variations of both surface potential and surface charge. Biogenic Hydroxyapatite (HAP) and one of its metastable precursors, a calcium dihydrogen phosphate dihydrate (DCPD) or Brushite were used to underline this resulting variation of chemical reactivity in zinc phosphates. In-situ monitoring of the transformation of Brushite in Hydroxyapatite is also reported.

Introduction

Hopeite is of considerable importance since it has been observed as a stable phase growing on the surfaces of zinc phosphate dental cements [1]. More recently great advances have been achieved in combining Hydroxyapatite (HAP) with zinc phosphate cements [2]. Accordingly, an implant with desired long term biostability and low cytotoxicity can be obtained in controlling the crystal size and the hydration state of zinc (ZP) and/or calcium phosphate containing materials [3–5]. Therefore many studies focus on the synthesis of biphasic zinc phosphate ceramics through various raw materials [6] and processes [7–8]. In addition retention of dental restoration to the tooth substance and sealing of the marginal gap between the restoration and tooth are dependent on the surface and bonding properties of ZP cements that critically control the adhesion stability and longevity of the restoration [9–12].

In the first part of this study, the thermal properties, the phases changes at certain temperatures and the resulting phase stabilities of zinc phosphate tetrahydrates were investigated using different thermal analysis techniques (differential scanning calorimetry-DSC, thermogravimetry-TGA-MS), combined with X-ray powder diffraction (XRD) and vibrational analysis (Diffuse Reflectance Infrared Fourier Transform-DRIFT, FT-Raman) [13]. It has been recently reported that zinc phosphate tetrahydrate has a greater tendency for dissolution and degradation than zinc phosphate dihydrate in an aqueous environment, which will decrease chemical stability and enhance degradation of ZP cements *in vivo* [14–17].

This current study was carried out with a view of elucidating aspects of the chemical stability and surface reactivity of ZP polymorphs, in comparison with Brushite (calcium dihydrogen phosphate dihydrate, DCPD) and Hydroxyapatite. The main focus has been to determine the chemical reactivity of the two forms of hopeite on short exposure to diluted H_3PO_4 and NH_4OH solutions and to correlate the obtained informations with the previously determined structural/bulk properties. Electron irradiation exposure may also give an estimation of the relative structural stability of brushite and hydroxyapatite. Further it is expected to provide basic information about the possible polymer-crystal surface interactions and beyond, to offer a starting point for future efficient modifications of zinc phosphate or hydroxyapatite based materials such as bone replacement cements [18].

*Author to whom all correspondence should be addressed.

Experimental

Synthesis

The synthesis of α-, β-zinc phosphate tetrahydrate (ZPT) and of calcium dihydrogen phosphate dihydrate (Brushite or CDPD) and Hydroxyapatite (HAP) as crystalline powders is described elsewhere [13].

Characterization

Scanning Electron micrographs (SEM) were taken with a LEO Gemini 1530 operated at 1 kV from a 35 ° angle side detector at a working distance of 5 mm.

For particle sizes and size distributions the powder was analysed by dynamic light scattering at 90 ° after ultrasonic dispersion for 10 min in a 10 wt% solution of non ionic surfactant (Lutensol AT50, BASF AG) and so-obtained statistics were compared with size distributions obtained from SEM images. Regarding the particle sizes and distributions determined from SEM images at least 250 crystals were measured per sample. To avoid errors due to projections of the three-dimensional crystal shape to a two-dimensional image, only crystals lying flat on the substrate were considered. Size histograms were calculated using a number based population balance approach [19] and fitted using Gaussian distributions [20].

Combined zeta-potential measurements were carried out by microelectrophoresis (Malvern Inst. Zetasizer 3000 HSA). Zeta-potential values were calculated from electrophoretic mobility data using the Helmholz-Smoluchowski equation with a f(KA) = 1.5, corrected by taking into account the particle size distribution of the powders (Henry equation). The aqueous dispersing behaviour was investigated through potentiometric titration. HNO_3 0.1 mol.L^{-1} and KOH 0.1 mol.L^{-1} were used to adjust the pH. The isoelectric point (IEP) was identified at the pH axis crossing point.

Results and discussion

Morphological studies

Fig. 1(a) and (b) show SEM micrographs of the α-and β-form of zinc phosphate tetrahydrate crystalline powders synthesized and used in this study. α-Hopeite crystals (Fig. 1(a)) present the classical plate shape and are reasonably uniformly sized of about 27 × 6 × 0.5 μm^3, whereas β-Hopeite crystals (Fig. 1(b)) were not as well defined and slightly smaller (24 × 5.5 × 0.5 μm^3) and

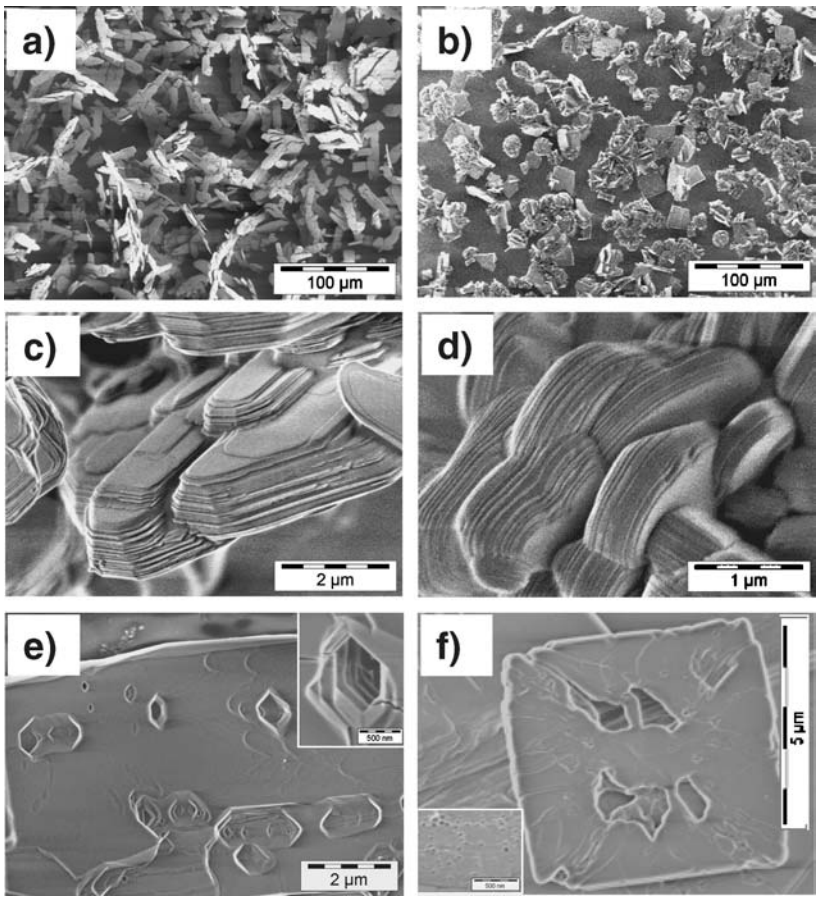

Figure 1 SEM photographs of: (a) α-hopeite, (b) β-hopeite. Chemical etching of: (c) α-hopeite, (d) β-hopeite in 0.1 M H_3PO_4 for 90 s at room temperature (with powder recovery by drying overnight in oven at 75 °C). Specific dissolution patterns are observed after 5 min immersion in 1 M NH_3 solution for α-hopeite in the [010] plane (e) and β-hopeite in the [011] plane (f).

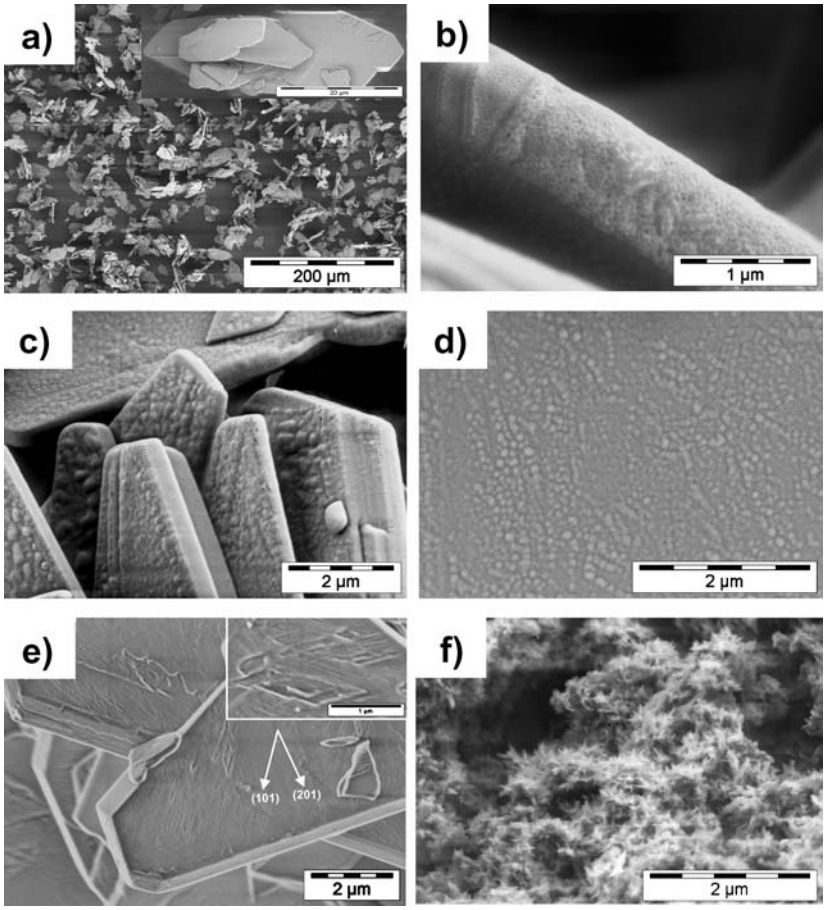

Figure 2 SEM photographs of Brushite: (a) after crystallization, characteristic needle-plate shape in inlet , (b) e-beam etching of pure Brushite for 60 s at 1.5 kV, (c) Chemical etching followed by e-beam irradiation (5 min, 3 kV), (d) periodically oriented OCP clusters on (010) brushite surface, (e) Trapezoidal etch pit in the *ac* plane obtained by immersion 1 M NH_3 solution, (f) needle like hydroxyapatite nanocrystals after precipitation at 40°C.

partially agglomerated (Fig. 3). The development of the faces of α-Hopeite crystals is sometimes irregular and the crystals may simulate hemimorphic symmetry. Comparingly the β-Hopeite sample presents two different habits: tabular {010} to prismatic {001}. This plate-like habitus of Hopeite crystal, whether α-form or β-form, corresponds to a layered structure, the *b*-axis being the crystal-plate normal [21]. A corresponding crystallographic representation is given in Fig. 4(a). In addition to growth SEM images of α- and β-Hopeite (Fig. 1(a) and (b)) suggest that secondary nucleation may occur with the appearance of small crystallites partially detached from the crystal surface, which continues to grow.

Fig. 2(a) shows twinned platelike crystals of brushite, with a shape similar to the one observed for the hopeite polymorphs. The insert in Fig. 2(a) illustrates a characteristic view of the {010} surface of a single crystal, which is the major growth and principle cleavage plane. Furthermore, the sequence of HAP formation suggests that the process, under the conditions used here, follows Ostwald's rule, according to which the formation of HAP, because of its high activation energy and its high thermodynamical stability, occurs via one or more metastable intermediate stage with low activation energy [22–23]. So as comparison to Brushite, the microstructural arrangement of tiny uniform crystals of Hydroxyapatite are also shown in Fig 2(d). Usually HAP crystallized from aqueous solution via precipitation at pH 11, forms a porous structure with blade shape, needle-like or rodlike crystallites of 200 nm in length and a maximum of 60 nm in width and height with no preferential direction of crystallite orientation. This morphology is obviously compatible with the results of Aosaka *et al.* [24]. But the formation of aggregates and the microchannel containing organization of HAP observed here may possibly originate from a spatial restriction due to the presence of organic tetramethylammonium hydroxide (TMAOH) as pH regulating agent in the mother liquor.

Fig. 3 displays compared crystal size distributions (CSD) of zinc and calcium phosphate hydrates. In many systems, particularly precipitation systems from zinc and calcium phosphate solutions agglomeration is an important factor and can not be overlooked. Unlike the simple case of α-Hopeite, which grows in two

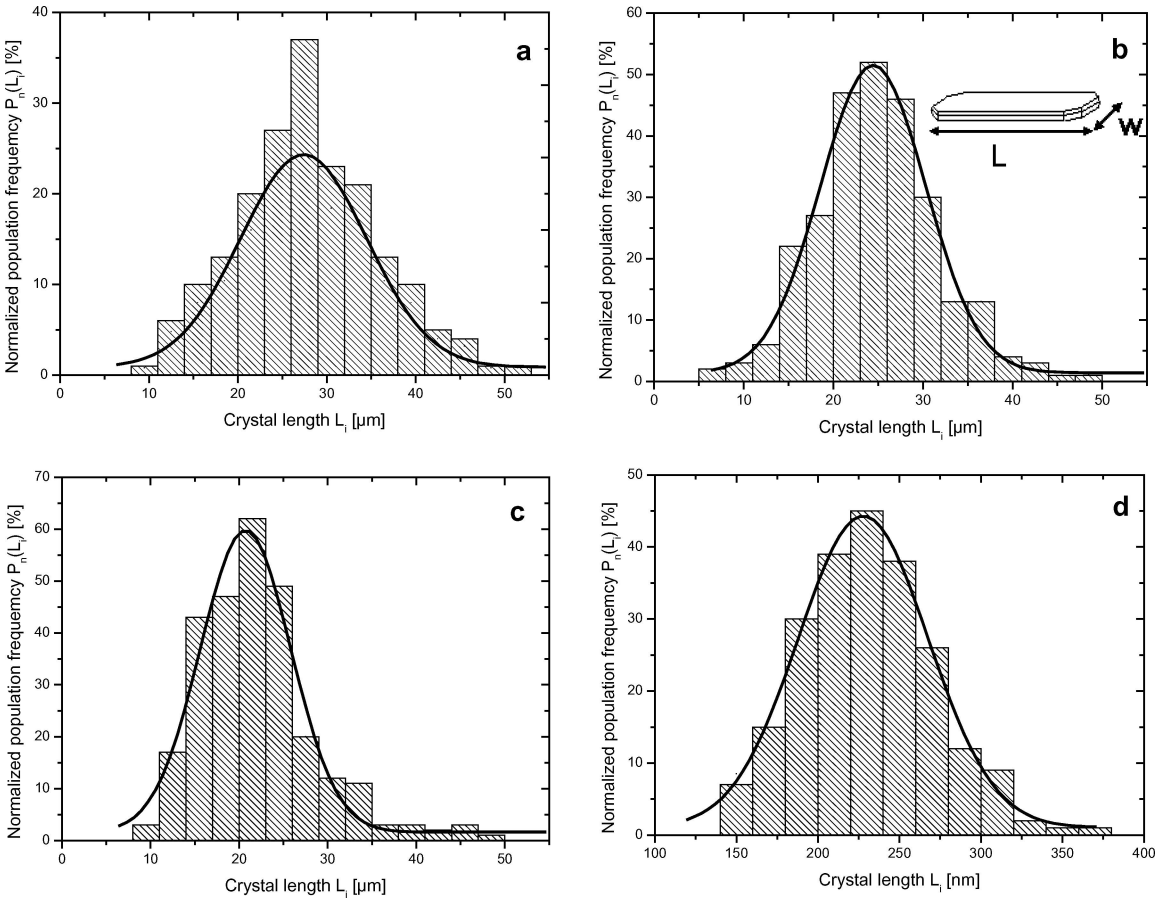

Figure 3 Size distribution histograms of model samples displayed in Figs 1 and 2: (a) α-hopeite, (b) β-hopeite, (c) brushite, (d) hydroxyapatite. Inset b shows the definition of crystal length L and crystal width w.

dimensions via a non-diffusion controlled mechanism [25] as shown in Fig. 1(a), it is necessary for β-Hopeite and Hydroxyapatite [26] (Figs 1(b) and 2(f)) to disregard a number-based CSD and use a particle size distribution based on volume or sphere population analysis [27–28]. It is presumed that these two last systems exhibit strong aggregation partially due to a strong heterogeneous nucleation or the presence of TMAOH in the specific case of HAP. These considerations are of primary importance since they justify the assumption made elsewhere [13], that since α-and β-Hopeite display similar dimensions, surface effects may be neglected for the determination of the thermodynamic parameters and interrelation between the different zinc phosphate hydrates.

Surface reactivity

There are only few reports on the relation between the surface chemistry and properties of zinc phosphate hydrates and their structural characteristics. Temptative explanations were given by Nancollas *et al*. for Brushite [29] and then by de Leeuw for Hydroxyapatite [30–31]. For instance, DFT calculations of Hydroxyapatite revealed that two energetically favoured configurations coexist, with preferred arrangement of hydroxyl groups, all OH^- groups being lined up with oxygen and hydrogen ions alternating in column parallel to the c-axis (Fig. 4(c)). These columns of aligned OH^- can of course be found in two directions, either up or down the c-axis, hence promoting a hydroxyapatite structure consisting of domains of well-ordered OH^- columns. A change in this ordering within these columns is possible either by thermal induction (only 42 kJ.mol^{-1} per OH group) or by the presence of anionic impurities (F^-, Cl^- , acrylate polymeric derivates). In order to obtain similar informations and also details about the stress induced crystal growth from a crystallographic point of view, in correlation with the surface reactivity and dissolution-reprecipitation mechanisms, the chemical etching of zinc phosphate and brushite crystals was investigated.

Putting ZPT crystals into a 1 up to 10 m mol.L^{-1} H_3PO_4 buffer solution of pH $\approx$ 2 time-dependent effects were observed and followed by scanning electron microscopy (Fig. 2(c) and (d)). During the first thirty seconds, no change in shape of the α-and β-ZPT crystals was observed, and the morphology was conserved

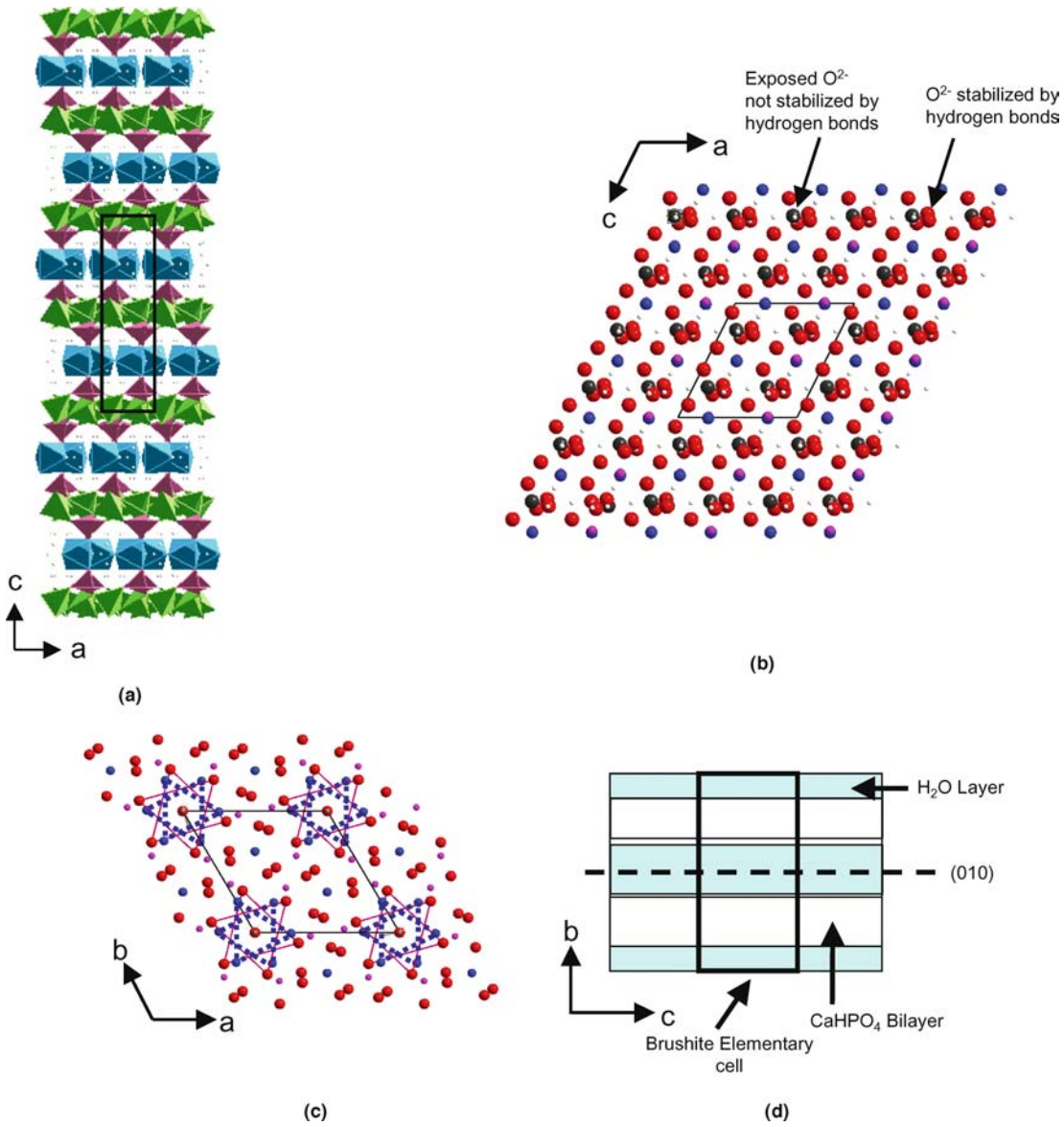

Figure 4 (a) Sheet arrangement of cation (Zn^{II})-centered polyhedra and phosphate tetrahedra in zinc phosphate tetrahydrate (hopeite). The framework is identical for α and β-hopeite. The connectivity is emphasized in projections along [010] (a). The green and magenta tetrahedra describe ZnO_4 (coodination 4) and PO_4 groups respectively. The blue octahedra are relative to the ZnO_6 (coordination 6) groups. (b) Crystallographic representation of Brushite showing a similar alternate layered structure as the Hopeite (blue: Ca, magenta: P, red: O, white: H) and emphasizing the orientation of phosphate hydrogen bonds along the *c*-axis, (c) Excerpt from the atomic structure of Hydroxyapatite illustrating the OH positions along the *c*-axis. Shown here are the columns of Ca (blue) and O (pink) involved in hydrogen bonding. (d) Schematic representation of Brushite viewed on the (001) plane, showing the water and $CaHPO_4$ bilayers along the *b*-axis.

except for a slight rounding of the edges. Fig. 2(c) and (d) show a characteristic "herringbone" texture in the (110) and (1$\underline{1}$0) faces corresponding to an alternating layered structure of zinc phosphate and water containing layers [32–33]. The local pH around these planes also changes with dissolution. This was evident with 1 m mol.L^{-1} H_3PO_4 buffer solution by adding a dye (bromocresol green) to the ZPT crystals maintained at pH $\sim$ 3. At this pH bromocresol green is of yellow colour. However the colour of the dye turned green as with dissolution started, in the vicinity of the lateral faces of both zinc phosphates, first indicating that the solution around these dissolving planes became more basic, and secondly proving the release of phosphate anions. This marks the disappearance of the monocrystalline character of the ZPT tetrahydrate platelets. If the local pH reaches 4, redeposition or "chemically induced" secondary nucleation takes place and the surface roughness softens [34]. In contrast, the (010) planes show no trace of dissolution in H_3PO_4. The absence of triangular etch pits on the flat terraces of the (010) surface shows that a homogeneous (hydrogen) bonding

environment exists [35–37]. This can be tested in immersing Hopeite crystals in 1 mol.L^{-1} NH_3 solution for 5 min (Fig. 1(e) and (f)). Already after a few seconds, α-Hopeite shows a specific quadratic dissolution pattern along the *a*- and *c*- axis, that transforms into an hexagonal shape after 5 minutes, due to truncations of the square summits in the {101} and {$\underline{1}0\underline{1}$} directions (angle of 45 $^\circ$ with *a* and *c*-intersects). In good agreement with Wolfe's observations [38], Fig. 1(e) emphasizes the fact that two preferential pitting orientations in the {100} and {001} directions coexist. Logically, β-Hopeite crystals have different dissolution behaviour (Fig. 1(f)). These crystals display occasional corrosion pits in the diagonals of the rectangular surfaces ([010] plane). Ammonia infiltrates in the sheets of β-Hopeite parallel to the *b*-axis and triggers triangular etch pits (intersection of (011) and (011) direction in *bc*-plane, insert Fig. 1(f)). From a crystallographic point of view, one should notice that each times, these corrosion pattern correspond point to point to one of the hydrogen bond direction, whether in the α-Hopeite or in the β-Hopeite.

Besides, more complex surface geometries are readily found in other metal phosphate crystals. While Brushite exhibits similar sheet crystal structures as α- and β-hopeite with alternating hydration and calcium phosphate layers (Fig. 2(a)), defect-free HAP displays a calcium phosphate framework (mirror planes) with hydroxyl groups perpendicularly alternating in columns, that do not form hydrogen bonds with adjacent orthophosphate groups [39]. Thus, after 2 min exposure to a 10 m mol.L^{-1} H_3PO_4 buffer solution, a slight striated morphology appears on the (110) and (1$\underline{1}$0) planes of Brushite crystals (Fig. 2(c)). None of the triangular etch pits bound by steps along {101} and {201} ((010) plane) mentioned by Ohta *et al*. [40–41] are found here, but a few are present only on the (401) lateral face, apparently along {001} (see insert Fig. 2(b)). This can be explained by the non- collinearity of oxygen pairs with the *c*-axis and their slight counter clockwise twisting from the {001} direction (preferential orientation of hydrogen bonds), which provides the lack of rotational symmetry necessary for the dissolution process [42]. Similarly, as above-mentioned, when attacked by ammonia α-Hopeite displays progressively trapezoidal and hexagonal pits, corresponding to a step-wise dehydration accompanied by an elementary rotation along the *c*-axis [43]. In that sense, it is possible to explain the controlled growth of thin apatite crystals with hexagonal symmetry on [010] of brushite [44]. This hypothesis is confirmed by the presence of characteristic trapezoidal etch pits (double triangular etch pits face to face along (201), (101) and (001)) in the *ac*-plane when brushite crystals are chemically attacked by 1 mol.L^{-1} NH_3 (Fig. 2(e))

Dramatic changes are observed when the (010) surface of brushite is exposed to a high energy electron beam as it occurs during Scanning Electron Microscopy (SEM), while the same surface of α- and β-ZPT crystals show a high stability (Fig. 1(a) and (b)). It was found that Brushite is a metastable precursor of Hydroxyapatite with a general tendency for the following transformation sequence under a broad range of conditions: Brushite $\rightarrow$ OCP $\rightarrow$ HAP, where OCP denotes the octacalcium phosphate phase [45–47]. Because of its platelike morphology (Fig. 2(a)) in the (010) orientation, the calcium phosphate dihydrate (Brushite) is suitable for e-beam etching. After 5 min exposure (induction period), the (010) surface show rise of periodically organised nanospherules (40 nm in diameter, Fig. 2(d)), forming a cluster-like morphology on further e-beam exposure (Fig. 2(c)). Similar results were achieved by Dickinson *et al*. [48] on exposure of the Brushite (010) surface to a 1–5 eV photon beam. Especially, correlated with the results of Posner *et al*. [38] and later with the interpretation of Nancollas and Mohan [49] for the transformation of amorphous calcium phosphate, we may speculatively identify this "freshly generated" phase as octacalcium phosphate. This would be the first experimental evidence of OCP growth on brushite surface caused by electron irradiation.

We support the idea that on exposure to an intensive electron beam on the SEM stage brushite heats locally ((010) plane) and hence dehydrates via HPO_4^{2-}condensation and crystal water release (partial leaking of hydrogen bonds) [50–51]. The Brushite surface becomes electroconductive and luminescent. The luminosity remanence ceased on stopping of the e-beam exposure [52]. In comparison, this electromolecular effect can not be observed for any of the hopeite polymorphs due to their higher thermodynamic stability. Subsequently in the [010] plane, oxygen radicals $O_2^{\bullet -}$ (superoxide anion radicals) are formed due to the presence of trapped electrons in the structure as reported successively by Monma *et al*. [53] and Kanai and coworkers [54–55]. This generates numerous structural atomic stresses with a depth of a few unit cells [56], necessary for the "epitaxial" growth of OCP islands on the (010) Brushite surface.

When there is a local lattice misfit of crystallographic parameters, the initially grown layers may display defects or imperfections inducing a less favourable direction for crystal growth.

The ability of one crystalline phase to grow on the surface of another is strongly dependent on the surface characteristics. The establishment of a defined orientation-relationship between the crystalline overgrowth and the substrate requires formation of at least one immobile monolayer of the building units of the new phase regularly organized on the nm-scale. It is suggested that there is a critical misfit threshold for an epitaxial monolayer in order to reach the same lattice spacing as the crystalline substrate [57–59, 43]. A generally accepted value is 10–20%, which is commonly known as the Royer-Friedel rule [60]. Turbull and Vonnegut

TABLE I Crystallographic data for Brushite and Octacalcium phosphate (OCP)

Structure name	Dicalcium phosphate dihydrate or Brushite (DCPD)	Octacalcium phosphate (OCP)
Crystal system	Monoclinic	Triclinic
Space group	$C2/_2$	$P\underline{1}$
a (Å)	5.812	19.625
b (Å)	15.180	9.629
c (Å)	6.359	6.830
α (°)	90.0	89.48
β (°)	118.52	92.68
γ (°)	90.0	107.48

[61] developed a global theory in which the efficiency of primary heterogeneous nucleation is also related to lattice matching, i.e. to lattice misfit δ, between nucleus and substrate and predicted that nuclei would most probably be created for values of δ below 0.015. Therefore, it is possible to consider the reactivity of the Brushite crystal surface in terms of lattice matching. Although brushite and octacalciumphosphate (OCP) crystallize in different systems, namely monoclinic and triclinic (Table I), both have a layered structure with alternating sheets of crystalline water and anionic tetrahedra of Ca^{2+} and PO_4^{3-}. While the "hydrated" layers of Brushite are oriented parallel to the (010) plane, the hydrated layers of OCP alternate with "apatitic" layers along the *a*-axis [62]. If one considers an epitaxial approach through a change of axis in the brushite *ac* plane, where {100} and {001} become {101} and {$\underline{1}$01} respectively, one can observe δ-values of 5.1 and 5.3% with the *b* and *c* lattice parameters of OCP. This indicates a remarkably close fit between both lattice structures. On the other hand, this misfit could be the reason for the change of the layer growth mode to the famous Stranski-Krastanov model describing the transition from layer to island growth. Following this model, heating by the electron beam increases the stored elastic energy in the nearest layers below the (010) surface. This elastic energy is then the driving force for the growth mode change. A strong support to this hypothesis comes from the presence of typical nanospherules and coalescing double-spheres of OCP, when the hydrated (010) faces of brushite crystals are exposed to an intensive electron beam (Fig. 2) [63].

From structural to surface properties

Another point to discuss is the influence of surface topology on the surface chemical stability or reactivity. This question can be efficiently approached by measuring the electrophoretic mobility of microcrystalline particles suspended in aqueous medium and thus obtaining the zeta-potential as a function of pH. The Smoluchowski equation [64] corrected for the effects of particle size distribution [65–66] and ionic strength of the suspension [67] are used in this context. It is an important observation that exposure to an electric field as well as stirring may initiate sedimentation and thus affect the overall stability of the suspension [68]. In consequence the large crystallite size of the brushite and hopeite polymorphs the presence of a non ionic surfactant (BASF, AT 50, C_{18}-$(CH_2$-CH_2-$O)_{51}H$) at constant ionic strength helped to evaluate the zeta-potential in delaying the destabilization of the suspension.

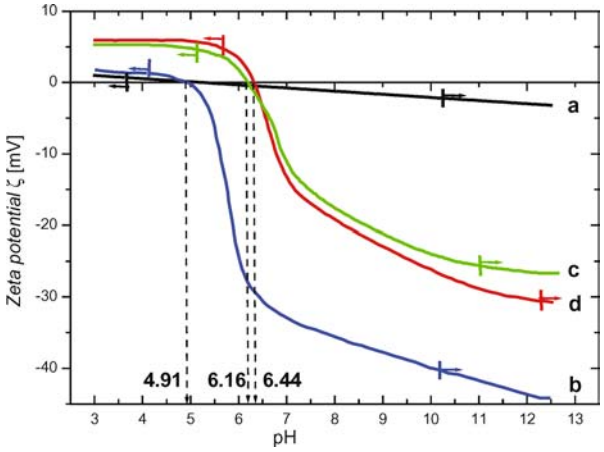

Figure 5 Effects of pH on zeta potential of (a) α-hopeite, (b) β-hopeite, (c) brushite, (d) hydroxyapatite at 25 °C under constant ionic strength (I = 0.05 M). Vertical lines and arrows indicate pH initiation of the solubilisation process.

The isoelectric point (IEP) of Brushite and Hydroxapatite occur at pH 6.16 and 6.44 respectively. This corresponds to reported values by Howie-Meyers [69] and Leach [70–72] as shown in Fig. 5. Under acidic conditions, a mixture of calcium deficient HAP, Monetite ($CaHPO_4$) or brushite will form as suggested by Brown [73]. Solubility diagrams for calcium phosphate [74] show that HAP may convert or at least coexist with brushite in an acidic environment at an approximate pH of 4.8. Below 4.8, Brushite and Monetite are the stable phases while above pH 4.8, HAP is the stable phase. In the light of the results mentioned by Lemaitre [75], the above measured IEP also correspond to vanishingly small concentration of free Ca^{2+} ions in the suspension and marks the onset of the precipitation reaction. Therefore at pH 6.9, the zeta-potential tends to stabilize Brushite and corresponds to its solubility minimum. However, at any given pH above of 4, Brushite exhibits a higher (30 orders of magnitude higher) solubility than HAP and similarly at pH above IEP a higher but negative zeta-potential [69]. In alkaline solution (pH > 9), a usual decrease of zeta potential followed by a plateau is attributed to dissolution of calcium phosphate, the release of Ca^{2+} in the aqueous medium, and the progressive adsorption of Na^+ at the dissolving surface (diffuse layer), mainly to compensate the buffering effect of surface phosphate groups (electroneutrality condition) [76].

There is no significant difference between IEP obtained for hopeite and calcium phosphate samples in

KCl, HNO_3, NaOH or $(CH_3)_4NOH$ solutions. As one would expect, the cation $(CH_3)_4N^+$ and the anion NO_3^- are to large to exchange with surface ions and, as there would be little tendency for these ions to form complexes with the surface ions, it is reasonable to assume that these ions behave indifferently and act only as counterion for any surface charge. It is not surprising therefore, that upon equilibration the zeta potential reflects partially the surface charge density. Rodrigues-Clemente *et al*. [77] show that citrate exchanges selectively with phosphate groups at the solid-solution interface, caused by a higher affinity of citrate than phosphate species for Ca-sites on HAP surface. This adsorption may take place via a bidentate surface-chelate interaction. Nevertheless, adsorption kinetics depends not only of surface chemistry but also on surface topology. For example, albeit α-and β-Hopeite have the same chemical composition and nearly the same particle size distributions, they display astonishing disparities in their electrophoretic behaviour.

Under acidic conditions, the conversion of both forms of Hopeite to zinc hydrogen phosphate (ZHP) (structure similar to Brushite) is very interesting as suggested by Nriagu [78] and is marked by a positive zeta-potential, independent of pH (pH $<$ 5), but below the IEP of 4.91. The isoelectric point is identical for α-and β-Hopeite. ZHP acts as a protective barrier and prevents complete dissolution of the hopeite core particles, as shown in the chemical etching test, by functioning as a semi-permeable layer. At IEP, the concentration of zinc ions in equilibrium with β-Hopeite is around 1 ppb and that with α-Hopeite is about 0.2 ppb ($pK_s = 44$ and 48). Therefore, this solubility difference appears to provide favourable conditions for bulk precipitation of β-Hopeite. In contrast surface conversion or surface precipitation is favoured in the case of α-Hopeite. While both Hopeite polymorphs display negative zeta potential above pH 5, the zeta-potential of α-Hopeite decreases linearly with pH in a unique manner, and reaches only -3.8 mV at pH 12. In contrast, β-Hopeite has already a high zeta potential up to -30 mV at pH 6.5. Above pH 7, the zeta-potential of β-Hopeite also decreases linearly with pH. Many factors may influence the zeta potential, but this linearity dependence with pH in basic medium may be explained in terms of dissolution-reprecipitation mechanism since at pH $>$ 6.3 zinc hydroxide tends to form and may adsorb on Hopeite surfaces [70, 79]. Furthermore, it is well known that sparingly soluble salt such as Brushite or Hopeite dissolve easily at high undersaturation, under the present conditions [37]. However, this can not explain the global difference of electrophoretic behaviour of α-and β-Hopeite. Ammonia and HNO_3 chemical etching experiments clearly suggest that surface potential and surface dissolution are correlated not only with the formation and propagation of etch-pits as described by the "self-inhibition" model of Nancollas *et al*. [80], but also with the surface morphology and insofar with the overall crystal architecture. In that sense, α-Hopeite possesses a three dimensional hydrogen bond network, inducing the formation of an isoenergetic layered structure (Fig. 4(a)) with an high surface tension γ_{SL} toward H_2O and ensuring a high surface stability against dissolution [81]. This hydrogen pattern inhibits the formation of etch-pits and prevents their preferential propagation along {010}. Consequently α-Hopeite display neutral or partially dissociated phosphate groups on the [010], [110] and [1$\underline{1}$0] planes, as reflected by a very low negative zeta-potential above pH 5. In contrast, because of an hydrogen bonding pattern oriented along the crystallographic *b*-axis, β-Hopeite displays under NH_4OH chemical etching a complete dissolution of all units in the [010] planes, exposing bare phosphate groups as indicated by a strong negative zeta-potential above pH 5. The [110] and [1$\underline{1}$0] planes are destabilized and etch pits can be specifically found on these planes.

Conclusion

In synergy with classical methods such as XRD, DRIFT, FT-Raman and Solid State NMR, which are mainly used for the characterization of bulk properties of microcrystalline powders of zinc phosphate hydrates, scanning electron microscopy offers an in-situ analysis of the particle morphology and size distribution. Besides, biological Hydroxyapatite (HAP) and one of its precursors (Brushite) were used to underline the resulting variations of surface chemical reactivity in zinc phosphates. Thanks to chemical etching and e-beam irradiation, combined with zeta-potential measurements, the first precise understanding of the surface stability of zinc phosphates was given in direct correlation with their unique structural properties. In addition, induced Brushite conversion to HAP by e-beam irradiation is reported for the first time. Further, this study may help design zinc phosphate cements with improved properties for advanced bioapplications.

References

1. G. E. SERVAIS and L. CARTZ, *J. Dent. Res.* **50** (1971) 613.
2. M. OTSUKA, S. MARUNAKA, Y. MATSUDA, A. ITO, P. LAYROLLE, H. NAITO and N. ICHINOSE, *J. Biomed. Mater. Res.* **52**(4) (2000) 819.
3. M. UO, G. SJOREN, A. SUNDH, F. WATARI, M. BERGMAN and U. LERNER, *Dent. Mater.* **19** (2003) 487.
4. A. PIWOWAREZYK and H. C. LAUE, *Oper. Dent.* **28**(5) (2003) 535.
5. A. ITO, H. KAWAMURA, M. OTSUKA, M. IKEUCHI, H. OHGUSHI, K. ISHIKAWA, K. ONUMA, N. KANZAKI, S. SOGO and N. ICHINOSE, *Mater. Sci. Eng. C –Bio.* S. **22**(1) (2002) 21.
6. A. D. WILSON and J. W. NICHOLSON, "Phosphate bonded cements", in "Acid-base cements: Their biomedical and industrial applications", edited by A. D. Wilson and J. W. NICHOLSON, (University Press, Cambridge, 1993).

7. W. W. BRACKETT and S. ROSEN, *Oper. Dent.* **19** (1994) 106.
8. J. LI, S. FORBERG and R. SöREMARK, *Acta. Ondotol. Scand.* **52** (1994) 209.
9. A. J. COLEMAN, H. H. D. RICKERBY and L. R. ANTONOFF, *Quintessence Int.* **32**(10) (2001) 811.
10. G. J. P. FLEMING, O. Narayan, *Dent. Mater.* **19**(1) (2003) 69.
11. M. M. PIEMJAI, *Int. J. Prosthodont.* **14**(5) (2001) 412.
12. R. NOMOTO and J. F. MCCABE, *Dent. Mater.* **17**(1) (2001) 53.
13. L. HERSCHKE, J. ROTTSTEGGE, I. LIEBERWIRTH and G. WEGNER, *J. Mater. Sci.: Mater. Med.* (accepted).
14. A. KALENDOVÁ and P. KALENDA, *Farbe + Lacke.* **109** (2003) 62.
15. J. W. NICHOLSON and M. A. AMIRI, *J. Mater. Sci.: Mater. Med.* **9**(10) (1998) 549.
16. E. J. VAN MILLER and K. L. DONLY, *Am. J. Dent.* **16**(5) (2003) 356
17. B. CZARNECKA, H. LIMANOWSKA-SHAW and J. W. NICHOLSON, *J. Mater. Sci.: Mater. Med.* **14**(7) (2003) 601
18. S. C. D'ANDREA and A.Y. FADEEV, *Langmuir.***19**(19) (2003) 7904.
19. A.S. MYERSON, "Handbook of industrial crystallization", 2nd Edition (Butterworth-Heinemann, NY, 2002), p. 101.
20. R.J. HUNTER, "Foundation of Colloid Science", (Oxford Science Publications, Oxford, 1986), Vol. 1 + 2.
21. O. V. YAKUBOVICH, O. V. KARMOVA, O. V. DIMITROVA and W. MASSA, *Acta. Cryst.* C**55** (1999) 151.
22. K. OTHA, M. KIKUCHI, J. TANAKA and H. EDA, *Key. Eng. Mat.* **240**(2) (2003) 517.
23. T. NISHINO, M. NAGAI, Z. SAKURAI and *et al.*, *J. Ceram. Soc. Jpn.* **104**(8) (1996) 729.
24. N. AOSAKA, S. BEST, J. C. KMOWLES and W. BONFIELD, "Characterization of HA precipitated from different reactants" in J. Wilson, L. L. Hench, D. Greenspan Editors, Bioceramics, Proceeding of the 8th International Symposium on Ceramics in Medicine, (Vol. **8**, Ponte Verda (FL) USA, Elsevier, 1995) p. 331.
25. L. PEREZ and G. H. NANCOLLAS, *J. Cryst. Growth.* **66**(2) (1984) 412.
26. N. M. HANSEN, R. FELIX, S. BISAZ and H. FLEISCH, *Biochim. Biophys Acta.* **451** (1976) 549.
27. R. W. HARTEL and A. D. RANDOLPH, *AiCHE J.* **32** (1986) 1136.
28. G. H. NANCOLLAS and J.A. BUDZ, *J. Dent. Res.* **69**(10) (1990) 1678.
29. A. HINA, G. H. NANCOLLAS and M. GRYNPAS, *J. Cryst. Growth.* **223** (2001) 213.
30. N. H. DE LEEUW, *Chem. Comm.* **17** (2001) 1646
31. N. H. DE LEEUW, *Phys. Chem. Chem. Phys.* **4**(15) (2002) 3865.
32. R. J. HILL and J. B. JONES, *Am. Mineralogist.* **61**(9/10) (1975) 987.
33. K. SANGWAL and K. W. BENZ, Prog. *Cryst. Growth and Charact.* **32** (1996) 135.
34. J. SAISON and J. J. TRILLAT, *Cr. Hebd. Acad. Sci.* **250**(13) (1960) 2374.
35. F. C. FRANK, *Acta Cryst.* **4** (1951) 497.
36. N. CABRERA, M. M. LEVINE and J. S.: PLASKETT, *Phys. Rev.* **96** (1954) 1153.
37. R. TANG, C. A. ORME and G. H. NANCOLLAS, *J. Phys. Chem.* B**107** (2003) 10653.
38. C. W. WOLFE, *Am. Miner.* **25**(12) (1940) 795.
39. A. S. POSNER, N. C. BLUMENTHAL and F. BETTS, in "Chemistry and structure of precipitated hydroxyl-apatites" in "Phosphate minerals", edited by J. O. Nriagu, P. B. Moore, (Springer-Verlag, Berlin, 1984) p.333.
40. M. OTHA, M. TSUTSUMI and S. UENO, *J. Cryst. Growth* **47** (1979) 135.
41. M. OTHA and M. TSUTSUMI, *J. Cryst. Growth* **56** (1982) 652.
42. L. SCUDIERO, S. C. LANGFORD and J. T. DICKINSON, *Tribol. Letters* **6** (1999) 41.
43. K. FLADE, C. LAU, M. MERTIG and W. POMPE, *Chem. Mater.* **13** (2001) 3596.
44. G. W. JOHNSON, *J. Appl. Phys.* **22** (1951) 797.
45. J. S. SØRENSEN and H. E. L. MADSEN, *J. Cryst. Growth* **216** (2000) 399.
46. E. A. P. DE MAEYER, R. M. H. VERBEECK and C. W. J. VERCRUYSSE, *J. Biomed. Mater. Res.* A**52**(1) (2000) 95.
47. (a) J. C. ELLIOTT, in "*Structure and Chemistry of Apatites and other Calcium Orthophosphates*", (Elsevier, Amsterdam, 1994); (b) G. Graham, P. W. Brown, *J. Cryst. Growth* **165** (1996) 106.
48. J. T. DICKINSON, C. BANDIS and S. C. LANGFORD, *Mat. Res. Soc. Symp.* **617** (2000) J1.1.1.
49. A. NANCOLLAS and M. S. MOHAN, *Arch. Oral. Biol.* **15** (1970) 731.
50. S. RÖßLER, A. SEWING, M. STÖLZER, R. BORN, D. SCARNWEBER, M. DARD and H. WORCH, *J. Biomed. Mater. Res* A**64**(4) (2003) 655.
51. H. MONMA, S. UENO, Y. TSUTSUMI and T. KANAZAWA, *Yogyo Kyokai-Shi* **86** (1978) 590.
52. X. LI, S. Q. GU, E. E. REUTER, J. T. VERDEYEN, S. G. BISHOP and J. J. COLEMAN, *J. Appl. Phys.* **80** (1996) 2680.
53. H. MONMA, S. UENO and T. KANAZAWA, J. *Chem. Technol. Biotechnol.* **31** (1981) 15.
54. Y. MATSUMURA, H. KANAI and J. B. MOFFAT, *J. Chem. Soc. Faraday Trans.* **93** (1997) 4383.
55. H. KANAI, Y. MATSUMURA and J. B. MOFFAT, *Phos. Res. Bull.* **6** (1996) 293.
56. D. L. VEZIE and E. L. THOMAS, *Polymer* **36**(9) (1995) 1761.
57. G. P. THOMSON, *Proc. Phys. Soc.* **61** (1948) 403.
58. J. H. VAN DER MERWE, *Discuss. Faraday. Soc.* **5** (1949) 201.
59. G. W. JOHNSON, *J. Appl. Phys.* **21** (1950) 1057.
60. H. AOKI IN "*Science and medical applications of hydroxyapatite*", (JAAS, Tokyo, 1991) p. 46.
61. D. TURNBULL and B. VONNEGUT, *Ind. Eng. Chem.* **44** (1952) 1291.
62. W. E. BROWN, J. P. SMITH, J. R. LEHR and A. W. FRAZIER, *Nature* **196** (1962) 1048.
63. A. BIGI, E. BOANINI, M. BORGHI, G. COJAZZI, S. PANZAVOLTA and N. ROVERI, *J. Inorg. Biochem.* **75** (1999) 145.
64. J. H. KENNEDY and A. FOISSY, J. *Am. Ceram. Soc.* **60**(1/2) (1977) 33.
65. Y. ZHANG, C. J. BRINKER and R. M. BROOKS, *Mater. Res. Soc. Symp. Proc.* **271** (1992) 465.
66. R. J. HUNTER, in "Zeta potential in Colloid Science: Principles and Applications" (Academic Press, New York, 1981) p. 11.
67. K. YAMASHITA, M. MATSUDA, Y. INDA, T. UMEGAKI, M. ITO and T. OKURA, J. *Am. Ceram. Soc.* **80** (1997) 1907.
68. E. V. KOROBKO, in "Proceedings of the Conference on Recent Advances in Adaptative and Sensory Materials and their Applications", edited by C.A. Rogers & R.C. Rogers Eds (Technomic, Blacksburg, Virginia, 1993) p. 3.
69. C. L. Howie-Meyers, D. L. Elliott, K. P. Ananthapadmanabhan, *Langmuir* **10** (1994) 320.
70. S. A. LEACH, *Arch. Oral. Biol.* **3** (1969) 48.
71. L. C. BELL, A. M. POSNER and J. C. P. QUIRK, *J. Colloids. Interf. Sci.* **42**(2) (1973) 250.
72. J. MA, C. H. LANG, L. B. KONG and C. WANG, *J. Mater. Sci.: Mater. Med.* **14** (2003) 797.
73. P. W. BROWN, *J. Am. Ceram. Soc.* **75** (1992) 17.

74. P. SOMASUNDARAN, J. O. AMANKONAH and K. P. ANANTHAPADMABHAN, *Colloids Surf.* **15** (1985) 309.
75. G. VEREECKE and J. LEMAITRE, *J. Cryst. Growth* **104** (1990) 820.
76. M. PRETTO, A. L. COSTA, E. LANDI, A. TAMPEIRI and C. GALASSI, *J. Am. Ceram. Soc.* **86**(9) (2003) 1534.
77. A. LÓPEZ-MACIPE, J. GÓMEZ-MORALES and R. RODRíGUEZ-CLEMENTE, *J. Colloids Interf. Sci.* **200** (1998) 114.
78. J. O. NRIAGU, *Geochim. & Cosmochim. Acta* **37** (1973) 2357.
79. SOLUBILITY DATA SERIES and EDITED BY IUPAC, (Pergamon, Oxford, 1979) p. 250.
80. R. TANG, C. A. ORME and G.H. NANCOLLAS, *J. Am. Chem. Soc.* **123** (2001) 5437.
81. A. E. NIELSEN, *Pure Appl. Chem.* **53** (1981) 2025.

Received 7 April 2004
and accepted 9 May 2005